White Matter Tractography Using Diffusion Tensor Deflection

Mariana Lazar,[1] David M. Weinstein,[2] Jay S. Tsuruda,[3] Khader M. Hasan,[4,8] Konstantinos Arfanakis,[4] M. Elizabeth Meyerand,[4] Benham Badie,[7] Howard A. Rowley,[6] Victor Haughton,[6] Aaron Field,[6] and Andrew L. Alexander[4,5,8]*

[1]*Department of Physics, University of Utah, Salt Lake City, Utah*
[2]*Department of Computer Science, University of Utah, Salt Lake City, Utah*
[3]*Department of Radiology, University of Utah, Salt Lake City, Utah*
[4]*Department of Medical Physics, University of Wisconsin, Madison, Wisconsin*
[5]*Department of Psychiatry, University of Wisconsin, Madison, Wisconsin*
[6]*Department of Radiology, University of Wisconsin, Madison, Wisconsin*
[7]*Department of Neurosurgery, University of Wisconsin, Madison, Wisconsin*
[8]*W.M. Keck Laboratory for Functional Brain Imaging and Behavior University of Wisconsin, Madison, Wisconsin*

Abstract: Diffusion tensor MRI provides unique directional diffusion information that can be used to estimate the patterns of white matter connectivity in the human brain. In this study, the behavior of an algorithm for white matter tractography is examined. The algorithm, called TEND, uses the entire diffusion tensor to deflect the estimated fiber trajectory. Simulations and imaging experiments on in vivo human brains were performed to investigate the behavior of the tractography algorithm. The simulations show that the deflection term is less sensitive than the major eigenvector to image noise. In the human brain imaging experiments, estimated tracts were generated in corpus callosum, corticospinal tract, internal capsule, corona radiata, superior longitudinal fasciculus, inferior longitudinal fasciculus, fronto-occipital fasciculus, and uncinate fasciculus. This approach is promising for mapping the organizational patterns of white matter in the human brain as well as mapping the relationship between major fiber trajectories and the location and extent of brain lesions. *Hum. Brain Mapping 18:306–321, 2003.* © 2003 Wiley-Liss, Inc.

Key words: diffusion tensor; tractography; tracking; streamlines; white matter

INTRODUCTION

Diffusion Tensor MRI (DT-MRI) may be used to characterize the orientational dependence of diffusion in a medium. In white matter (WM), the measured diffusion of water appears to be greatest along the fiber direction and more restricted in the perpendicular direction. Connectivity between different brain re-

Contract grant sponsor: National Institute of Health; Contract grant numbers: P30 CA42014, MH62015.

*Correspondence to: Andrew L. Alexander, Ph.D., W.M. Keck Laboratory for Functional Brain Imaging and Behavior Waisman Center, 1500 Highland Ave., University of Wisconsin, Madison, WI 53705-2280. E-mail: aalexander@waisman.wisc.edu

Received for publication 2 April 2002; Accepted 13 January 2003
DOI 10.1002/hbm.10102

gions may be estimated from the long-range continuity in the diffusion tensor field, and it is believed to be correlated to the underlying white matter fiber systems [Basser et al., 2000; Conturo et al., 1999; Jones et al., 1999; Le Bihan et al., 2001; Poupon et al. 2000; Stieltjes et al. 2001]. A path of connection between two brain regions is constructed by starting from a voxel and inferring continuity from voxel to voxel [Le Bihan et al., 2001], using an estimate of local tract direction. Recent studies have attempted to reconstruct the apparent patterns of white matter tracts in both the human brain [Basser et al., 2000; Conturo et al., 1999; Jones et al., 1999; Poupon et al. 2000; Stieltjes et al. 2001; Tench et al., 2002] and the mouse brain [Mori et al., 1999] using DT-MRI. These WM tractography results are promising for the non-invasive estimation of brain structural connectivity. For example, the relationship between fiber trajectories and the position of brain lesions may be important for characterizing neurological symptoms and predicting therapeutic outcomes.

Most current tractography methods use the major DT eigenvector to define the local fiber direction. This approach appears to work well in many instances; however, there are a few potential limitations in this method that should be considered. First, image noise will influence the direction of the major eigenvector leading to directional error accumulation in the estimated fiber tracts [Anderson, 2001; Basser et al., 2000; Lazar and Alexander, 2001; Lazar et al., 2001; Lori et al., 2000]. Second, as the degree of anisotropy decreases, the uncertainty in the major eigenvector increases, which means that tracking may be erroneous in regions where the DT does not appear to have strong directional component, such as the thalamus, and association white matter (e.g., the arcuate fasciculus, the pons, and subcortical WM) [Alexander et al., 2000]. Third, tractography may also be affected by partial voluming effects [Alexander et al., 2001; Tuch et al., 1999; Wiegell et al., 2000]. A white matter tract is defined as a group of nerve fibers with a consistent pathway [Heimer, 1995]. Tracts do not always form ''well-defined bundles,'' since the fibers of neighboring pathways often interconnect. A distinct collection of nerve fibers is referred to as either a fasciculus, a peduncle, or a brachium. These collections of fibers often contain multiple tracts [Heimer, 1995]. The measured voxel size in DT-MRI (dimensions of 1–4 mm on a side) is much greater than the size of the nerve fibers (dimensions of microns). In regions of coherent fiber directionality such as the trunk of tracts or fascicles, of dimensions larger or comparable to the voxel size, the major eigenvector of the diffusion tensor will approximate the local tract direction [Basser and Pierpaoli, 1996]. In regions where fibers are crossing, merging, or fanning, the measured diffusion data represent a complex averaging of multiple compartments within a voxel. However, the major eigenvector cannot adequately describe the direction of two or more intersecting tracts simultaneously.

In this study, the properties of a white matter tracking approach are investigated. The technique, called tensor deflection, uses the entire tensor to determine the direction of tract propagation, instead of just the major eigenvector direction. Some of the properties of tensor deflection are presented in comparison with a recently described streamlines approach [Mori et al., 2000]. Results of white matter tracking in both normal subjects and a patient with a brain neoplasm are presented. Finally, advantages and disadvantages of the algorithm are presented and strategies for improvement are discussed.

Abbreviations

ADC	apparent diffusion coefficient
CL	linear tensor shape measure
CP	planar tensor shape measure
DT	diffusion tensor
FA	fractional anisotropy
FACT	fiber assignment by continuous tracking
STT	streamlines tracking
TEND	tensor deflection
WM	white matter

THEORY

The diffusion tensor, D, defines a principal frame of directions for each voxel by its eigenvectors. The diffusion displacement profile may be represented as an ellipsoid with the principal axes lengths related to the tensor eigenvalues (principal diffusivities: λ_1, λ_2, and λ_3) and the directions given by the tensor eigenvectors ($\mathbf{e}_1$, $\mathbf{e}_2$, and $\mathbf{e}_3$). The major eigenvector ($\mathbf{e}_1$), corresponding to the direction of greatest diffusivity, is assumed to give the fiber direction in white matter regions. Based on this directional information, different methods and algorithms have been proposed to estimate white matter connectivity.

Streamline tracking

Streamlines tracking (STT) techniques model propagation in the major eigenvector field of the brain [Basser et al., 2000; Conturo et al., 1999; Mori et al., 1999]. The major eigenvector direction is assumed to be tangent to the tract pathway. This approach is

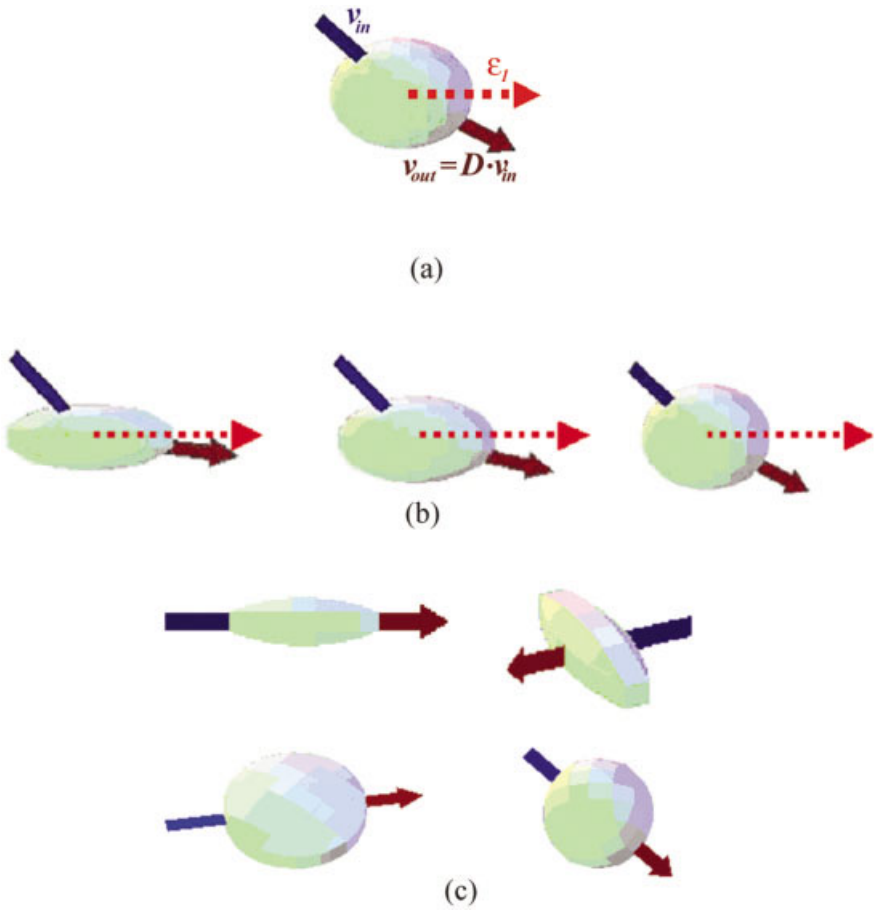

Figure 1.

a: Illustration of tensor deflection (TEND) for a cylindrically symmetric diffusion tensor. Incoming vector: blue; deflected vector: dark red; major eigenvector: dashed red. **b:** Illustration of TEND as function of the tensor shape. For more anisotropic tensor (left) the incoming vector is deflected toward the major eigenvector. The amount of deflection decreases with decreasing anisotropy (from left to right). **c:** Illustration of four cases where TEND will not cause any vector deviation. These cases include the incoming vector being either parallel or perpendicular to the major eigenvector of a cylindrically symmetric tensor ellipsoid, in the plane of a oblate tensor ellipsoid, or in any orientation for a spherical ellipsoid.

analogous to simulated flow propagation in fluid dynamics [Helman and Hesselink, 1991], including the study of blood flow phenomena from MRI flow measurements with 3-D phase contrast [Buonocore, 1994; Napel et al., 1992].

Tensor deflection

An alternative approach for determining tract direction is to use the entire DT to deflect the incoming vector ($\mathbf{v}_{in}$) direction [Weinstein et al., 1999]:

$$\mathbf{v}_{out} = \mathbf{D} \cdot \mathbf{v}_{in} \quad (1)$$

The incoming vector represents the propagation direction from the previous integration step. The tensor operator deflects the incoming vector towards the major eigenvector direction, but limits the curvature of the deflection, which should result in smoother tract reconstructions. This algorithm is called TEND for tensor deflection. Figure 1 illustrates the TEND algorithm deflection properties for diffusion ellipsoids having different shapes.

In the TEND algorithm, the incoming vector, $\mathbf{v}_{in}$, can be conveniently described by using a linear combination of the three DT eigenvectors:

$$\mathbf{v}_{in} = \alpha_1 \mathbf{e}_1 + \alpha_2 \mathbf{e}_2 + \alpha_3 \mathbf{e}_3, \quad (2)$$

where α_1, α_2 and α_3 are the relative vector weightings. By multiplying both sides of Eq. 2 by **D**, substituting

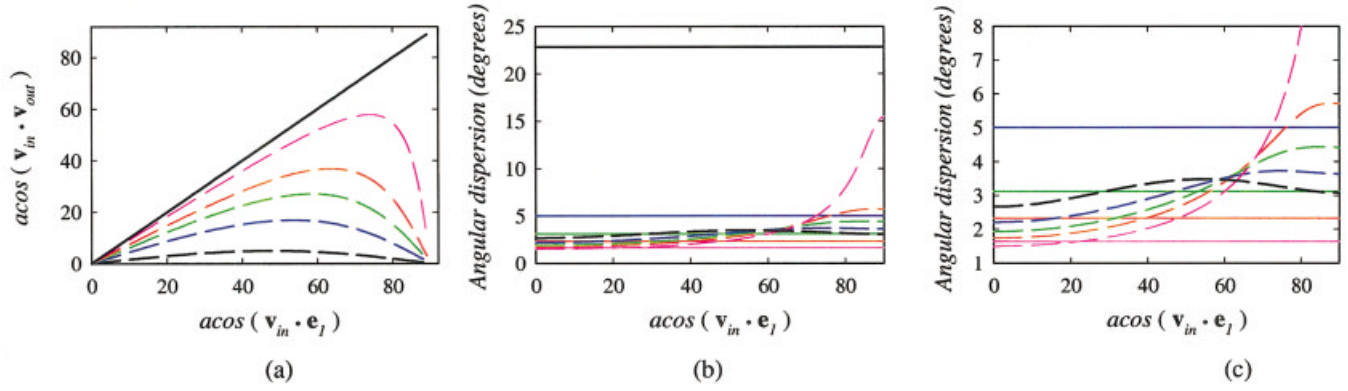

Figure 2.

a: The deflected angle, acos($\mathbf{v}_{in} \cdot \mathbf{v}_{out}$), as a function of the angle between the incoming vector and tensor major eigenvector direction, acos($\mathbf{v}_{in} \cdot \mathbf{e}_1$), for five FA levels (0.10, black; 0.36, blue; 0.55, green; 0.70, red; 0.91, magenta). The tensor is assumed to be cylindrically symmetric. The deflection angle decreases with lower anisotropy and is zero for both the parallel and perpendicular orientations. TEND: dashed line; STT: solid line. **b:** Angular dispersion for STT (solid lines) and TEND (dashed lines) for a signal-to-noise ratio of 50 for the same FA levels as described in a. **c:** Same as b with a smaller horizontal axis range to highlight differences in the TEND plots.

$\lambda_i \mathbf{e}_i$ for $\mathbf{D}\mathbf{e}_i$ (the characteristic matrix equation), and normalizing to the largest eigenvalue, Eq. 1 can be rewritten as:

$$\mathbf{v}_{out} = \lambda_1 \left(\alpha_1 \mathbf{e}_1 + \frac{\lambda_2}{\lambda_1} \alpha_2 \mathbf{e}_2 + \frac{\lambda_3}{\lambda_1} \alpha_3 \mathbf{e}_3 \right) \qquad (3)$$

Note that $\mathbf{v}_{out}$ is an unscaled vector whereas $\mathbf{e}_1$, $\mathbf{e}_2$, $\mathbf{e}_3$ are unit vectors. Several specific cases are described here. If the incoming vector coincides with one of the tensor eigenvectors, all α's will be zero except the one corresponding to the eigenvector direction and $\mathbf{v}_{in}$ will not be deviated by tensor (e.g., $\mathbf{v}_{out} = \mathbf{v}_{in}$ Fig. 1c, top row). The degree of tensor deflection is plotted in Figure 2a as a function of the DT anisotropy (for cylindrically symmetric DT's) and the angle between $\mathbf{v}_{in}$ and $\mathbf{e}_1$.

For a highly prolate DT (e.g., $\lambda_1 >> \lambda_2, \lambda_3$), and α_1 not much less than α_2 or α_3, the output vector of the TEND algorithm will be deflected towards the direction of the major eigenvector, $\mathbf{v}_{out} = \lambda_1\alpha_1\mathbf{e}_1 + \Delta \approx \lambda_1\alpha_1\mathbf{e}_1$. However, for $\alpha_1 << \alpha_2$ or α_3, the tract direction will not be highly deflected.

For an oblate shaped DT (e.g., $\lambda_1 \approx \lambda_2 \gg \lambda_3$) and α_3 small, the deflected vector is $\mathbf{v}_{out} \approx \lambda_1(\alpha_1\mathbf{e}_1 + \alpha_2\mathbf{e}_2)$. In this case, both the major and medium eigenvectors contribute most heavily to the deflection. The incoming vector component perpendicular to the tensor plane (defined by $\mathbf{e}_3$) will be attenuated so that the incoming vector will be deflected toward the ellipsoid plane. This behavior may be desirable for voxels with planar diffusion where eigenvector degeneracy can occur and the direction of fastest diffusivity is not well defined. The planar tensor shape may appear in regions with crossing, fanning, or merging fibers [Alexander et al., 2001; Wiegell et al., 2000]. However, when $\mathbf{v}_{in}$ is roughly in the $\mathbf{e}_3$ direction, the incoming vector will be relatively undeflected.

For an isotropic tensor (e.g., $\lambda_1 \approx \lambda_2 \approx \lambda_3$), the incoming vector will not be significantly deviated, $\mathbf{v}_{out} \approx \lambda_1(\alpha_1\mathbf{e}_1 + \alpha_2\mathbf{e}_2 + \alpha_3\mathbf{e}_3) \equiv \mathbf{v}_{in}$.

The tensorline algorithm

In the brain, it is expected that the measured diffusion tensor field will be heterogeneous. Consequently, it may be sensible to use STT for highly prolate DT voxels, and to use TEND when the DT has a more oblate or spherical tensor shape. The original tensorlines algorithm, described by Weinstein et al. [1999] dynamically modulates the STT and TEND contributions to tract steering:

$$\mathbf{v}_{out} = f\mathbf{e}_1 + (1-f)((1-g)\mathbf{v}_{in} + g\mathbf{D} \cdot \mathbf{v}_{in}), \qquad (4)$$

where f and g are user-defined weighting factors that vary between 0 and 1. The algorithm has three directional terms: (a) an $\mathbf{e}_1$ STT term weighted by f, (b) a TEND term ($\mathbf{D} \cdot \mathbf{v}_{in}$) weighted by $(1\text{-}f)g$, and (c) an undeviated $\mathbf{v}_{in}$ term weighted by $(1\text{-}f)(1\text{-}g)$. The vectors $\mathbf{e}_1$, $\mathbf{v}_{in}$ and $\mathbf{v}_{out}$ are normalized to unity before being used in Eq. 4. Estimated trajectories with different properties can be achieved by changing f and g. Consequently, tensorlines may be considered as a

family of tractography algorithms that can be "tuned" to accentuate specific behavior. In the original implementation of this algorithm, Weinstein et al. [1999] used a measure of prolate tensor shape, $f = CL$ [Alexander et al., 2000; Kindlmann et al., 1999; Westin et al., 1999], to weight the STT term. Note that for $f = 1$, the tensorlines algorithm is equivalent to STT.

Tract propagation

Several stepping methods for discrete tract propagation have been described. Mori et al. [1999] developed the FACT (Fiber Assignment by Continuous Tracking) algorithm, which alters the propagation direction at the voxel boundary interfaces. Consequently, the FACT algorithm uses variable step sizes, depending upon the length of the trajectory needed to pass through a voxel. An alternative procedure described by Conturo et al. [1999] uses a constant step size (CSS) approach for propagating the fiber tract. Recently, Basser et al. [2000] described a method for estimating the continuous tensor field and dynamically varying the step size as a function of the tract curvature. For all approaches, the step size must be small relative to the curvature of the trajectory.

Seeding and terminating tracts

The estimated tracts are generated by seeding specified brain regions [Basser et al., 2000; Mori et al., 1999] and following them until termination. Another strategy starts by seeding large regions of the brain, followed by selecting tract groups that cross a specified region of interest [Conturo et al., 1999]. Stopping criteria include tensor voxels with an anisotropy value below a specific threshold [Basser et al., 2000; Conturo et al., 1999], or the local curvature of the reconstructed fiber exceeding a critical value [Basser et al., 2000; Xue et al., 1999]. The first criterion will stop the propagation of the computed tract when it reaches regions where a fastest diffusivity direction is not well defined. The curvature criterion will inhibit the trajectories from following unlikely pathways.

METHODS

Simulation of tensor deflection behavior

The tensor deflection operation in Equation (1) bends the propagation vector, $\mathbf{v}_{out}$, towards the major eigenvector direction. This means that for relatively straight pathways, the dispersion in the TEND algorithm should be less than for STT. To test this hypothesis, a Monte Carlo (MC) simulation was used to evaluate the effects of image noise on the deflected direction described by Equation (1). The diffusion weighted signals were calculated for a specified diffusion tensor shape and orientation with respect to $\mathbf{v}_{in}$, for and ideal non-diffusion-weighted signal (b = 0) with a signal intensity of 1,000 units. Gaussian random noise was added to baseline and diffusion weighted signals (similar to MC experiments described by Pierpaoli and Basser [1996]). The standard deviation of the noise was 20 units (e.g., SNR = 50). The noise experiment was repeated 4,000 times and the angular dispersion was calculated. The angular dispersion was defined as the average angular error from the noise-free direction. A range of anisotropic tensors (all cylindrically symmetric) from FA = 0.1 to 0.9 was investigated. FA is a normalized (ranges between 0 and 1), rotationally-invariant measure of tensor anisotropy [Basser and Pierpaoli, 1998].

Diffusion tensor imaging

DT-MRI of three presumed normal subjects and one patient with a primary brain tumor were obtained either at the University of Wisconsin (UW) or the University of Utah (U of U). Informed consent was obtained from the subjects in accordance with the guidelines of the Institutional Review Board for human subject studies at the corresponding institution. Images were obtained using 1.5 tesla SIGNA scanners (General Electric Medical Systems, Milwaukee, WI) with Cvi gradients (40 mT/m, 150 mT/m/msec). At both institutions, a conventional single-shot spin echo EPI pulse sequence was modified to obtain diffusion-weighted (DW) images from any arbitrary set of specified diffusion-weighting directions.

One normal subject (Subject 1) at the UofU was studied using a six-directional encoding scheme described by Basser et al. [1998]. Other imaging parameters were TR = 5,000 msec, TE = 78.4 msec and a b value of 995 sec/mm^2. The acquisition for each encoding direction was repeated seven times for magnitude averaging. Axial images (2 mm thick) were acquired to cover a 3-D brain volume, $256 \times 256 \times 160$ mm^3, the latter dimension in the S/I direction). The original voxel size was $2 \times 1 \times 2$ mm^3, which was interpolated to $1 \times 1 \times 1$ mm^3 isotropic dimensions. The acquisition was repeated 8 times with 10 slices (20 mm wide) per series (~4:10 min each) to achieve the desired coverage (each volume was imaged twice with a 1-mm shift in the slice direction). The total imaging time was roughly 45 min.

At UW, two normal subjects (Subjects 2 and 3) and one brain tumor patient (Subject 4) were imaged with 23 diffusion-tensor encoding directions, which were generated with a minimum energy optimization algorithm [Hasan et al., 2001]. The imaging parameters were TR = 4,500 msec, TE = 71.8 msec, 4 NEX (image magnitude averaging on the scanner) and a b-value = 1,000 sec/mm^2. Axial images (3 mm thick) were acquired to cover a 3-D brain volume: 240 × 240 × 117 mm^3). The original voxel size was 1.87 × 1.87 × 3.0 mm^3, which was interpolated to 0.94-mm isotropic dimensions. The acquisition was split into two volume acquisitions of 20 slices because of image number limitations on the scanner. The top volume coverage went from the most superior aspect of the brain to the midbrain. The bottom volume covered from the most inferior slice of the top volume to the brain stem. Each slab required 7 min 30 sec to acquire (15 min total scan time).

Diffusion tensor image reconstruction

Image misregistration from motion and eddy current distortion was corrected using a 2-D linear registration algorithm in AIR (Automated Image Registration) [Woods et al., 1998]. The two diffusion tensor slabs were combined into a single 3-D volume. Overlapping slices between the slabs were used to ensure good coregistration between the slab volumes. For the data set from U of U, median filtering (3 × 3 kernel, in axial plane) was applied to each diffusion-weighted image to improve the image signal-to-noise. The combined single volume slab was interpolated to isotropic voxel dimensions.

White matter tracking with TEND

All processing of the data (tensor calculations and tracking) was performed using code developed at both the University of Utah and the University of Wisconsin in IDL (Research Systems, Boulder, CO). First the tensor measurements were diagonalized [Hasan et al., 2001a]. Maps of the diffusion tensor elements, ADC (= trace{D}/3), FA, CL, CP, and major eigenvector direction were calculated for the volume.

The TEND tracking algorithm used in this study employs the FACT algorithm described by Mori et al. [1999] as the stepping method. The propagation direction at each step is given by the deflection vector. Tract seeding is performed either by selecting a seed region on a 3-D diffusion tensor map (e.g., the FA map) or by seeding every voxel in the brain above a specified FA threshold (e.g., FA > 0.4). In both cases, only one seed was placed at the center of each voxel that was part of the specified region of interest. The major eigenvectors of seed voxels were selected as the original propagation directions. The tract is propagated both in the forward and reverse directions of the major eigenvector. The FACT algorithm used here alters the trajectory at the intersection of the voxel boundaries. At each new voxel, the propagation direction is calculated using Equation (1). Unless otherwise specified, tracts were terminated when FA became less than 0.2 or when the change in the direction exceeded 45 degrees. Tracking was performed in major commisural, projectional, and association WM pathways for each subject. Comparative results between STT and TEND are presented for corpus callosum and projection fibers.

The course of many white matter structures has been well documented in anatomic studies [Gluhbegovic and Williams, 1980; Heimer, 1995; Krieg, 1966; Riley, 1960]. The nomenclature of the fiber tracts and cortical areas used here is based on Heimer [1995] and Gluhbegovic and Williams [1980]. The trunk of different white matter structures has been previously identified using color maps obtained with DTI [Makris et al., 1997; Mori et al, 2002; Pajevic and Pierpaoli, 1999]. For most of the white matter structures investigated here, the estimated white matter trajectory was selected using labeled regions of interest that correspond to known white matter structures on the anisotropy, eigenvector color maps, or T2-weighted images.

RESULTS

Simulation of tensor deflection behavior

The deflected angle, acos($\mathbf{v}_{in} \cdot \mathbf{v}_{out}$), as a function of the angle between the incoming vector and tensor deflection direction, acos($\mathbf{v}_{in} \cdot \mathbf{e}_1$), is plotted in Figure 2a for five levels of FA. For more highly anisotropic tensors, the deflection direction approximates the major eigenvector direction for a broad range of tensor orientations, but falls off rapidly as the orientation of the tensor to $\mathbf{v}_{in}$ approaches 90 degrees. Conversely, for more isotropic tensors, the tensor deflection is fairly independent of the tensor orientation.

The angular variation or dispersion as a function of the image noise was also estimated. The dispersions in both the deflected directions (dashed lines) and the major eigenvector directions (solid lines) as a function of the tensor orientation with respect to the incoming vector direction are plotted in Figure 2b and c. The dispersion in the major eigenvector direction (solid lines) is independent of the incoming vector direction and increases with lower anisotropy. The plots also show that TEND dispersion is lower than the corresponding major eigenvector dispersion for a parallel

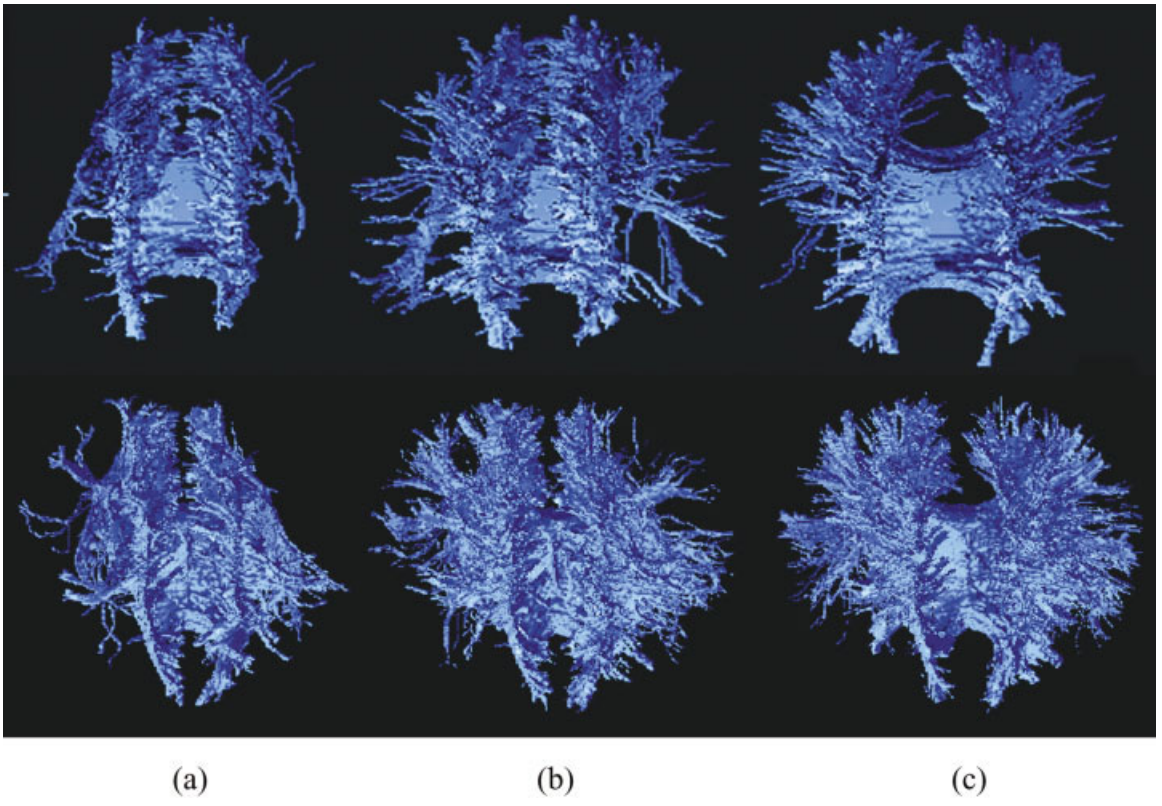

Figure 3.

Fibers of corpus callosum (Subject 1, top row; Subject 3, bottom row). The pathways were seeded on the midline of the corpus callosum in the sagittal plane. The fiber trajectories were terminated if they reached regions with FA lower than 0.15 or if the angle between two consecutive steps was larger than 45 degrees. The voxels intersected by estimated fiber trajectories were labeled and the resulting volume was rendered. Different tract reconstructions were obtained using **a:** STT, **b:** TEND, **c:** tensorlines (Equation (4) w/ $f = 0$, $g = 0.3$). **c:** illustrates that a combination of deflection and incoming vector resulted in fibers that connect more lateral regions of the two hemispheres.

tensor orientation (0 degrees). The TEND dispersion becomes much greater for highly anisotropic tensors as the orientation becomes more oblique. As expected, the dispersion is relatively independent of orientation for more isotropic tensors.

Human brain white matter tractography

Commissural pathways

The majority of interhemispheric pathways are in the corpus callosum (CC), which has the highest anisotropy and moderate curvature. A comparison of corpus callosum tract estimates that were generated using TEND, STT, and a combination of TEND and STT defined by Equation (4) is shown in Figure 3 for Subjects 1 and 3. The apparent tracts were generated by seeding a region situated at the midline of the corpus callosum, and covering few adjacent sagittal slices. A FA map was used to separate corpus callosum from the surrounding tissue. Generally, tracking using STT or deflection resulted in fibers curving and running up toward the cingulate cortex (Fig. 3a). These results are similar to those obtained by Basser et al. [2000]. By increasing the weighting of the incoming vector in Eq (9), the estimated pathways emerge from the region of intersection with corona radiata at a lower position and reveal connections between more lateral regions of the two hemispheres (Fig. 3b and c). Note that both medial cortex and lateral cortex callosal pathways have been observed by fiber dissection studies [Gluhbegovic and Williams, 1980; Riley, 1960].

Projection pathways

The connections between the cerebral cortex and the spine, including the corticospinal tracts, are a part of

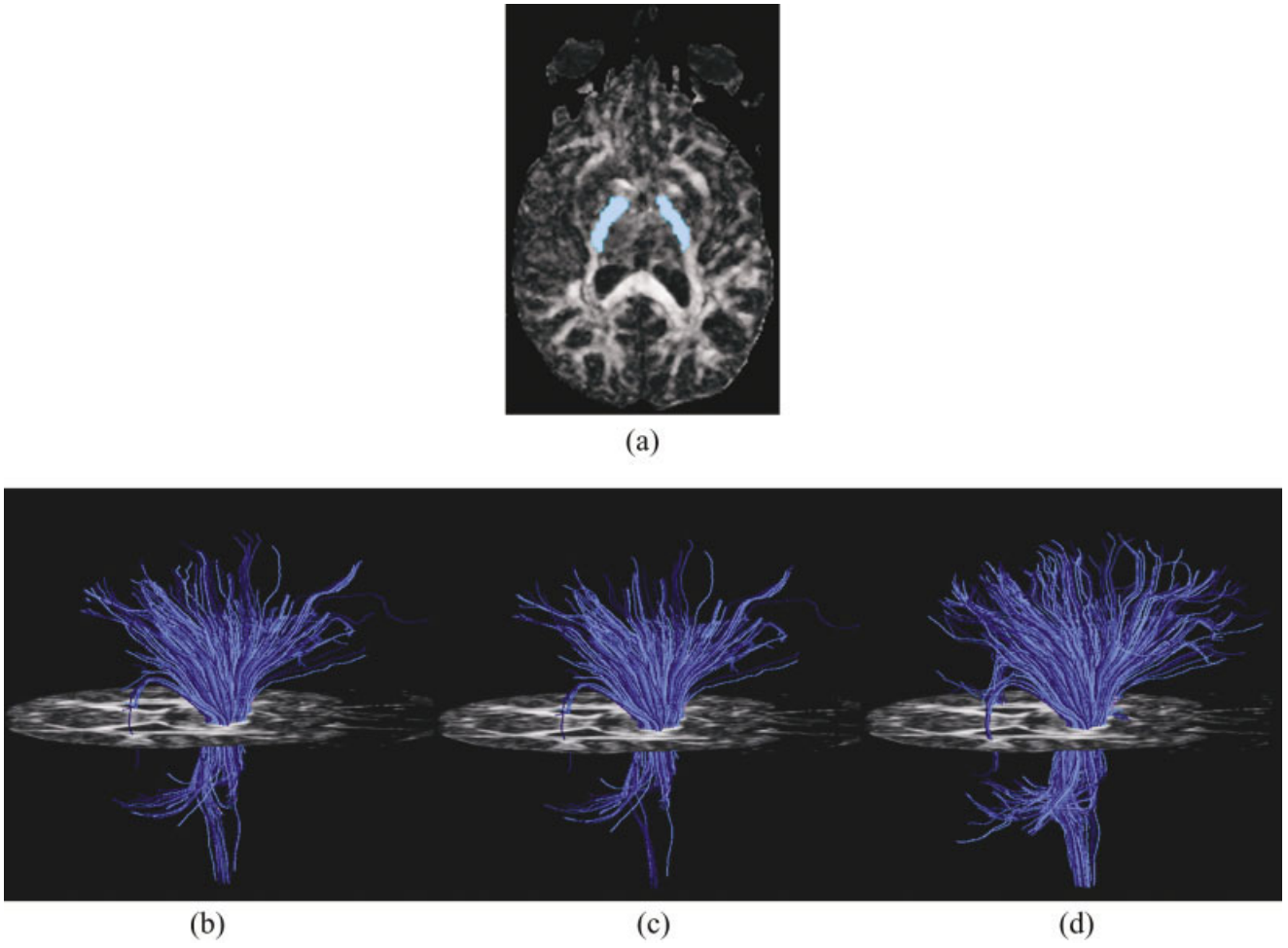

Figure 4.
STT vs. TEND for fibers of the internal capsule (Subject 1). **a:** seeding region (light blue) overlaid over FA map; **b:** STT, for an threshold angle of 45 degrees, average tract length 76.1 mm; **c:** STT, for an threshold angle of 36 degrees, average tract length 66.4 mm; **d:** TEND, for an threshold angle of 45 degrees, average tract length 117.7 mm. The average tract length when using TEND, for a threshold angle of 36 degrees remains 117.7 mm (image similar to d).

the projection fibers system. They pass through the internal capsule and form the corona radiata.

In order to compare TEND and STT algorithm behavior for fibers of internal capsule, estimated fibers pathways were generated from a small region of interest (Fig. 4a) using both STT and TEND. Two threshold angles were investigated: 45 degrees and 36 degrees. The results are presented in Figure 4b–d. The TEND pathways propagated further than the STT tracts for both thresholds. Whereas the decrease in the angular threshold from 45 degrees to 36 degrees resulted in shorter STT fibers, it did not affect the TEND trajectories. This result is consistent with the simulation results in Figure 2, which show that the TEND algorithm demonstrates reduced curvature and sensitivity to image noise. When the angular criterion for terminating the pathways is completely omitted, a large number of STT trajectories show bizarre tract behavior, sharp bends and loops, whereas the TEND trajectories generally did not.

Estimates of cortico-spinal tract (CST) and projection fibers of the internal capsule, obtained using TEND, are illustrated in Figures 5 and 6, respectively. For all the subjects, CST was obtained by seeding the entire brain and selecting the fibers emerging from the motor cortex and reaching the basis pedunculi. Results are presented for Subjects 1 and 3. The estimated CST pathways propagate inferiorly through the internal capsule. At the level of the pons, some branches split into the cerebellum and spinal tract. Tracts of the

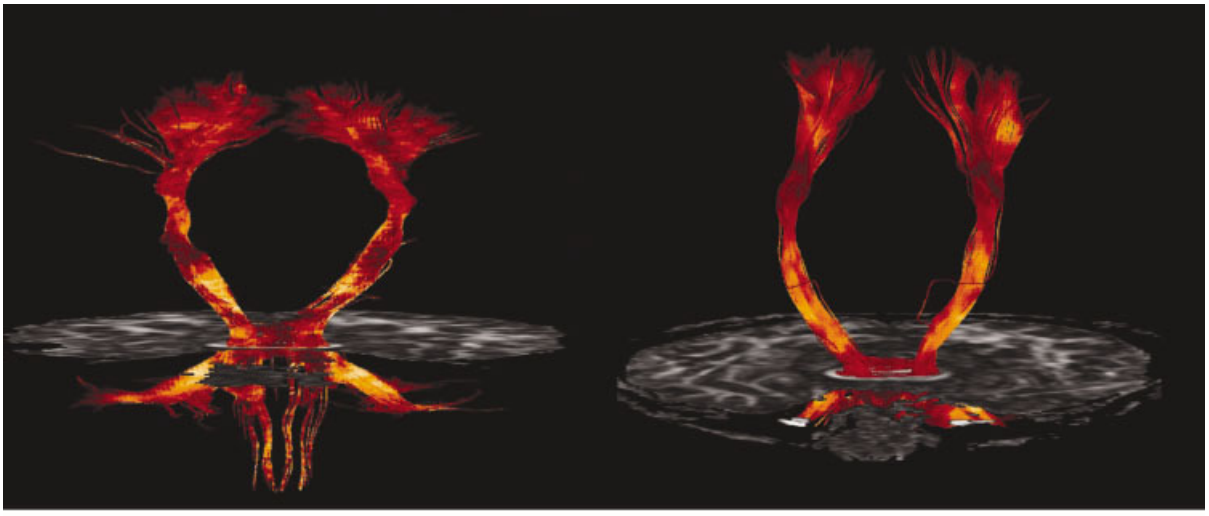

Figure 5.
Fibers of corticospinal tract. **a:** Subject 1. **b:** Subject 3. TEND trajectories were generated from white matter regions situated in motor and sensory cortex. The fibers reaching the basis pedunculi were retained. The coloring corresponds to the anisotropy (yellow = high vs. red = low anisotropy).

internal capsule were obtained by seeding medial portions of the cerebral cortex on both hemispheres. The tracts of internal capsule were selected in a horizontal section (axial plane) situated about halfway through thalamus in the inferior-superior direction. Different portions of the internal capsule have been parsed and labeled with a specific color (Fig. 6). This enables the user to follow pathways from a specific region to other regions of the brain. The separation of apparent tracts accordingly to the cortical region was not the original intent of the parsing; however, an approximate color mapping could be distinguished: yellow, frontal cortex; blue, pre-SMA (PSMA); orange, supplementary motor area (SMA); green, motor cortex; purple, sensory cortex; pink, visual cortex. The estimated motor pathways as seen in the axial and the sagittal planes present a good correspondence to the known anatomy [Heimer, 1995]. Note that this color mapping of the internal capsule was not repeated for all subjects, the only set of tracts that were not.

Association pathways

The tracts of the superior longitudinal fasciculus (SLF), inferior longitudinal fasciculus (ILF), inferior fronto-occipital fasciculus (IFOF), and uncinate fasciculus (UNC) are responsible for many intra-hemispheric connections within the brain. Estimates for these pathways are shown in Figure 7 for two different subjects. Fiber trajectories were generated from each voxel of the brain with a fractional anisotropy greater than 0.45. The tract groups were selected using hand-drawn regions-of-interest (ROIs) in coronal cross-section similar to Mori et al. [2002]. The placement of the selection ROIs was performed as consistently as possible across subjects and in both hemispheres.

The SLF (for both left and right hemispheres) was estimated by selecting white matter cross-sections in coronal anisotropy color maps (e.g., analogous to the procedure described by Mori et al. [2002]). In this plane, the SLF (also called the arcuate fasciculus) appears as a triangular green region (green indicates fibers in the anterior/posterior orientation) and also has a fairly high planar anisotropy [Alexander et al., 2000]. In addition to the SLF, several projection and commissural pathways were also observed intersecting the tract-selection region of interest (ROI). The projection and commissural tracts were selected and removed from the SLF results presented in Figure 7 (indicated as blue fibers).

The other association fiber pathways were estimated by placing two selection ROIs regions situated in coronal cross-sections (e.g., similar to Mori et al. [2002]) for each association group. The two ROIs correspond to the different regions of the brain that the fasciculi connect (e.g., occipital and frontal lobes for

IFOF, temporal and occipital lobes for ILF, frontal and temporal lobes for UNC). Note that this approach retains the longest pathways of the fasciculi, but it may omit some of the shorter pathways that do not travel the entire distance.

Generally, the trends for each of the pathways estimated for each subject were very similar; however, the identical branching and extent behaviors of these association tracts were not observed across all individuals, nor even across hemispheres. For example, the SLF in Figure 7b does not extend as far into the frontal lobe as it does on the contralateral side (Fig. 7a). Conversely, the pre-frontal tracts in the IFOF and the UNC appear to extend more anterior in Figure 7a than in Figure 7b. The CST estimate for Subject 1 appears to fan more near the motor cortex than the estimates for Subject 2 (Fig. 5). The variations in tract behavior are likely to be a combination of variations in anatomy, and image noise. An investigation of these issues is being performed.

Tractography in a tumor patient

The SLF pathways were estimated bilaterally on a 24-year-old male with a glioma in the left frontal lobe and a history of seizures (Fig. 8). The estimated SLF tracts on the right (contralateral) side appeared consistent with the pathways observed on the normal subjects. On the left (ipsilateral) side, the SLF appeared to run into the lesion and stop. This stopping at the lesion boundary was caused by the low FA (< 0.2) within the tumor margin. A lower FA threshold may have showed some tracts entering into the lesion. Close visual inspection of the cross-sectional DT-MRI images (FA and color eigenvector maps) showed some directional anisotropy within the lesion, which may indicate viable white matter pathways within the tumor.

DISCUSSION

In this study, the use of tensor deflection for estimating the organizational patterns of white matter structures was investigated. The tensor deflection operator approach (e.g., Equation (1)) for tractography was first described by Weinstein et al. [1999] and Westin et al. [1999]. Weinstein et al. [1999] showed preliminary tracking results in cingulum bundles (upper portion) and sparse regions of corona radiata and sagittal stratum. Westin et al. [1999] showed only simulation results. Subsequently, Lazar et al. [2000] compared tensorlines tractography with FACT streamlines [Mori et al., 1999] in corona radiata and cortico-spinal tract and found that the tensorlines tracts were smoother and generally showed less sharp bends in the tracts. Both Westin et al. [1999] and Lazar et al. [2000] showed, using simulations, that deflection was able to propagate tracts through perpendicular pathway intersections, which was not possible with streamlines. The ability to "plow through" regions of tract intersections is promising, but doesn't work as well when the tracks are not perpendicular. The simulations by Lazar et al. [2000] showed that oblique tracts could be crossed by using more of the undeviated term in Equation (4). Obviously, the problem of crossing fiber pathways in one or more voxels remains a challenge to characterize properly. This study presents a more complete analysis of the TEND algorithm than the original tensorline review of Weinstein et al. [1999]. A theoretical framework for interpreting the algorithm behavior as a function of the tensor shape and tract history has been introduced and the stability of the deflection vector with respect to noise is analyzed.

In tracking the corpus callosum, TEND and, more generally, tensorlines in Equation (4) were able to reconstruct pathways connecting upper cingulate cortex and superior frontal gyrus as well as more lateral hemispheric regions. Previous corpus callosum tracking results with STT methods [Basser et al., 2000; Mori et al., 1999] have only shown the most medial connection pathways, which are consistent with our STT results. The reason that most STT results do not show lateral connections is that the area near the intersection of corpus callosum, internal capsule, and superior longitudinal fasciculus shows a decreased anisotropy and directional ambiguity because of fibers crossing within single voxels. The TEND algorithm, however, is able to cross regions with low anisotropy better than STT.

Similar tracking results were observed across individuals with TEND, although a rigorous comparison was not performed. Recent studies by Stieltjes et al. [2001] and Mori et al. [2002] have started to evaluate the repeatability of the STT algorithm with FACT in the brainstem and in the association pathways. Their results demonstrate good reliability with their algorithm. A similar rigorous multiple subject analysis with TEND is planned for future studies.

Whereas the similarity of results obtained across different subjects increases the confidence in the performance of tractography algorithms, it does not guarantee the accuracy of the individual fibers estimates. Generally, a tract trunk is comprised of coherent fiber bundles (provided that it is not crossed by other major tract), which will facilitate a better performance of the tracking algorithms. The dispersion of fibers as they

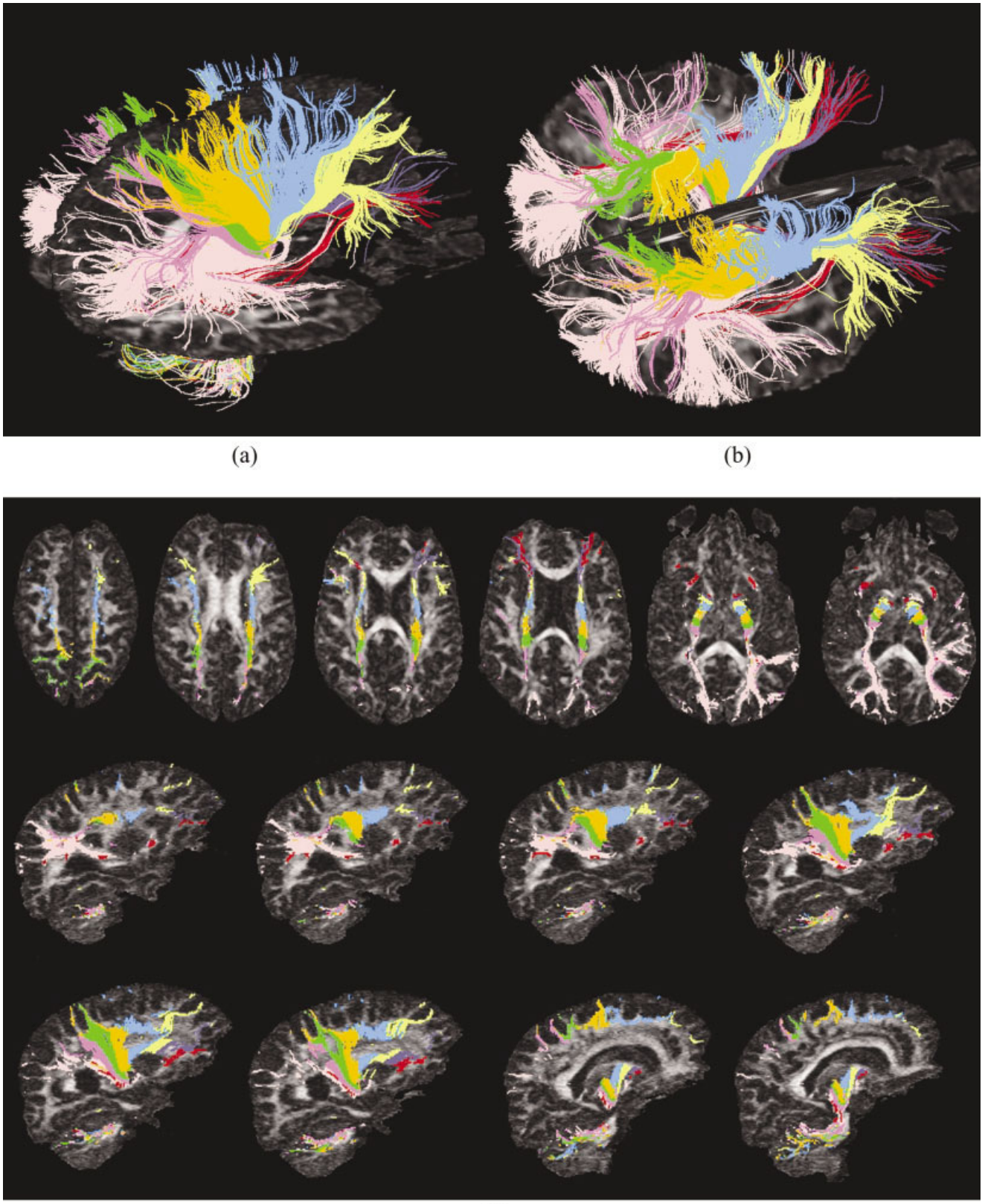

Figure 6.

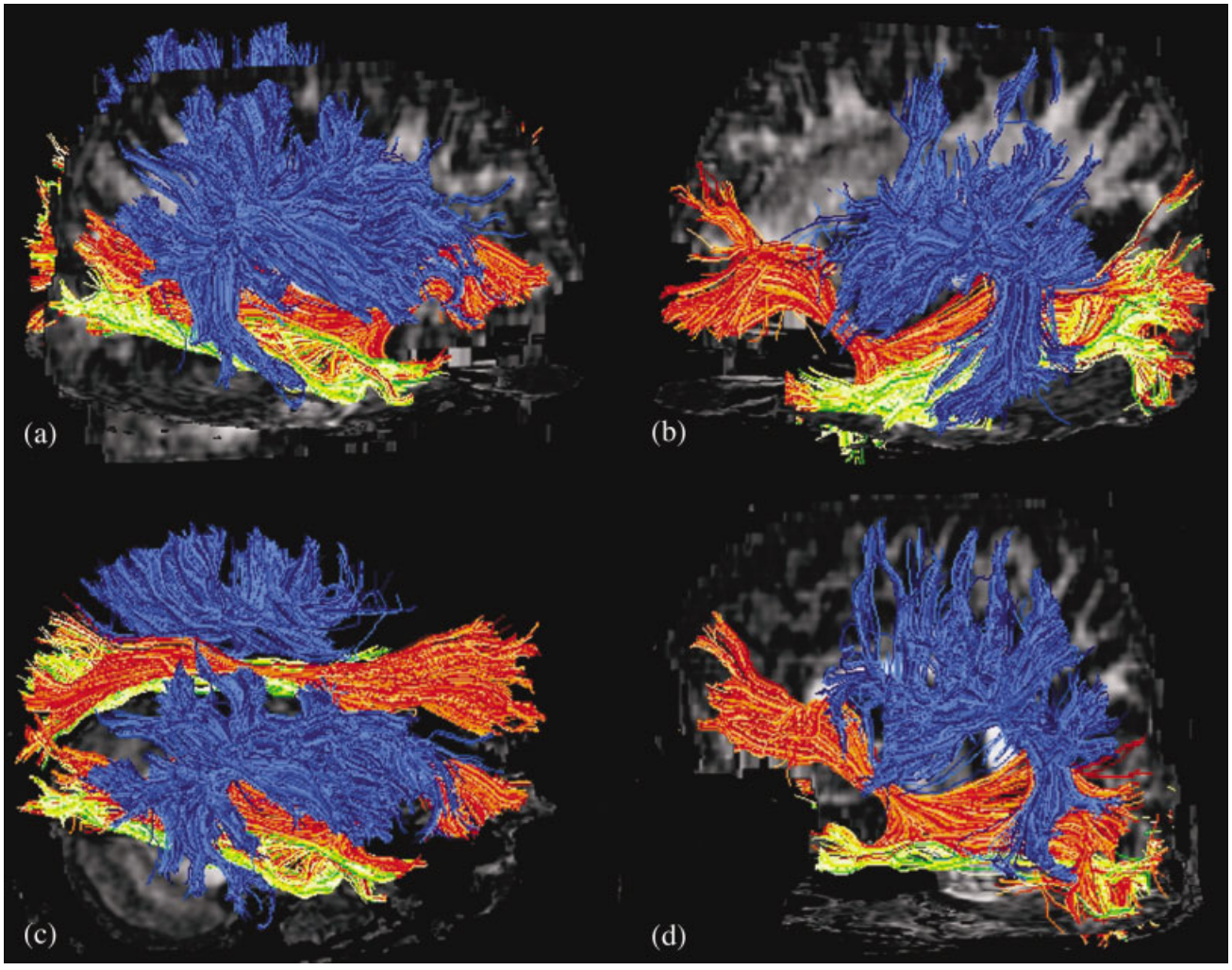

Figure 7.

Association pathways: Superior longitudinal fasciculus (blue), fronto-occipital fasciculus and uncinate fasciculus (orange), inferior longitudinal fasciculus (green-yellow). **a–c:** Subject 2, right and left hemispheres. **d:** Subject 3. All the pathways were obtained using the TEND algorithm and are similar to those obtained using STT by Mori et al. [2002].

join or leave the tract trunk may influence the accuracy of individual fiber terminations. In comparisons of different tracking parameters in Equation (4), we found that the main trunks of the tracts were consistent for a wide range of algorithmic parameters, but branching behavior varied significantly (data not shown). A primary cause of variability in branching behavior is thought to be caused by small variations in the tractography algorithm behavior, which can lead to large apparent variations in estimated tract behav-

Figure 6.

Projection fibers (corona radiata) reconstruction (Subject 1). The fibers were parsed and color-coded according to their anterior-posterior position in the internal capsule. **a,b:** Two rendered views of the parsed pathways. **c:** Axial and sagittal cross-sectional images. Although similar, there are slight bilateral variations due to imperfections in the region selection (by hand) and asymmetries in the brain. The color encoding enables the simultaneous visualization of different fibers groups. Most of the fibers project upwards into the corona radiata and reach different regions of the cortex. In the inferior direction, the fibers propagate toward brainstem where a large number reach the cerebellum and others propagate towards the spine. Note that when fibers from more than one group cross the same voxel, only the last path painted will appear, resulting in a painting artifact.

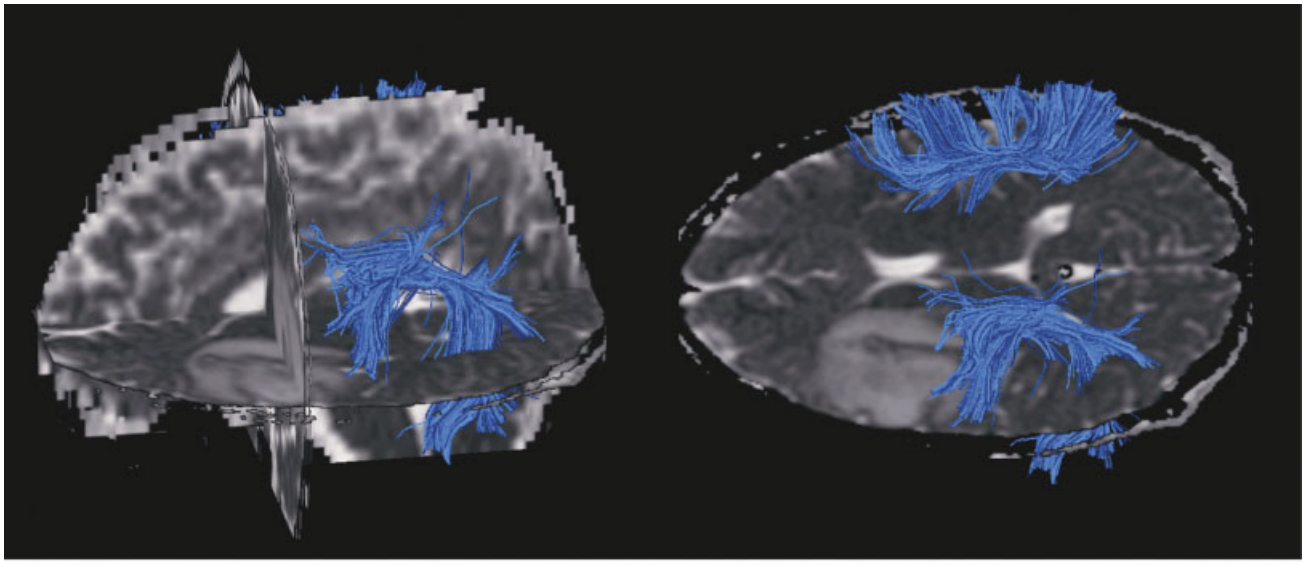

Figure 8.

Superior longitudinal fasciculus tracking in a patient with a left frontal oligodendroglioma (Subject 4). The estimated tracts are superimposed over ADC maps. **a:** Side view. **b:** Partial top view. Similar appearance to the SLF in normal subjects is observed on the contralateral side. On the ipsilateral side, the SLF pathways appear to terminate at the tumor periphery. Close examination of the anisotropy and eigenvector images show some preserved directional anisotropy within the tumor although it is below the anisotropy stopping threshold for the tracking algorithm.

ior near the edges of the trunk (e.g., once a tract has left the trunk, its behavior will be unique).

Most tractography algorithms (including both STT and TEND) are likely to work reasonably well in simple, organized, and homogeneous white matter regions such as corpus callosum, especially when the image SNR is sufficiently high. However, the white matter in the human brain appears to have fairly complex organization that can be confounded by partial volume effects. The voxel sizes used in DT-MRI are much larger than the white matter structures that are being mapped, leading to significant partial volume errors. For voxels with partial voluming, the major eigenvector represents, at most, an averaged direction of the contained tissues, and in the worst case, measurements that violate the diffusion tensor model [Alexander et al., 2001; Tuch et al., 1999; Wiegell et al., 2000]. In general, the volume averaging will decrease the tensor anisotropy. In low anisotropy regions, TEND will maintain a lower curvature trajectory relative to STT, because the major eigenvector directions are not well defined for the low anisotropy voxels. The use of smaller voxels will reduce the partial volume effects, but this will also decrease the image signal-to-noise. The use of higher dimensional diffusion measurements [Tuch et al., 1999; Wedeen et al., 2000] may be useful for detecting and characterizing multiple tracts in a single voxel.

The fundamental difference between TEND and STT is that TEND uses the entire diffusion tensor to

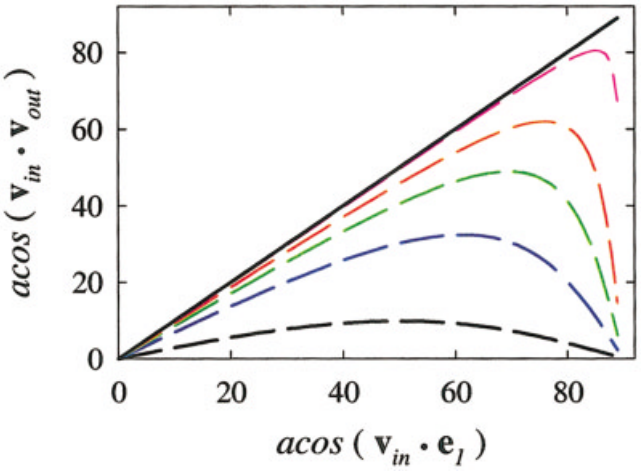

Figure 9.

The deflected angle, acos($\mathbf{v}_{in} \cdot \mathbf{v}_{out}$), for second order TEND, as a function of the angle between the incoming vector and tensor major eigenvector direction, acos($\mathbf{v}_{in} \cdot \mathbf{e}_1$), for the same FA levels as in Figure 2. TEND, dashed line; STT, solid line.

determine the direction of propagation. In straight pathways, the TEND algorithm is much less sensitive to both measurement noise and lower tensor anisotropy than the STT algorithm (Fig. 2). However, TEND will underestimate the trajectory curvature for curved pathways. This error is cumulative, but can be reduced by using smaller step sizes. Consequently, there is a tradeoff between lower error with the TEND algorithm in straighter sections, but higher systematic errors in curved sections. One approach to balancing this tradeoff is using a combined STT and TEND algorithm such as Equation (4). Recent simulations of tractography in noisy, homogeneous tensor fields (straight, helical, and circular) showed that the TEND algorithm displayed less error than the STT for either low SNR DT-MRI measurements or low tensor anisotropy [Lazar and Alexander, 2001]. However, the tensor fields of curved trajectories with high anisotropy and sufficiently high measurement SNR were more accurately represented using STT.

The discrepancy between the major eigenvector direction and the deflected direction can be reduced by applying the deflection operator 2 or more times,

$$\mathbf{v}_{out}^{(n)} = \mathbf{D}^n \mathrm{v}_{in} \tag{5}$$

where n represents the number of tensor multiplications. The higher order deflection can be expanded to a similar expression to that of Equation (3):

$$\mathbf{v}_{out}^{(n)} = \lambda_1^n \left(\alpha_1 \mathbf{e}_1 + \left(\frac{\lambda_2}{\lambda_1}\right)^n \alpha_2 \mathbf{e}_2 + \left(\frac{\lambda_3}{\lambda_1}\right)^n \alpha_3 \mathbf{e}_3 \right) \tag{6}$$

As the power n increases, the ratio terms λ_j/λ_1, $j = 2,3$ in Equation (6) will become smaller, provided that both λ_2 and λ_3 are smaller than λ_1. Consequently, $\mathbf{v}_{out}^{(n)}$ will converge toward $\mathbf{e}_1$ as n increases. This is reflected in Figure 9, which shows the deflected vector dependence for $n = 2$. Equation (5) also provides some insight into the behavior for TEND in the case of a small step size (either continuous or variable) integration. TEND will converge towards STT for very small step sizes, since more deflections will be applied as the incremental distance is decreased (i.e., more steps are nearly equivalent to increasing n in Equation (5)). The exception is in the case when the incoming trajectory is nearly perpendicular to the tensor. In this case, the deflection will remain relatively small.

The algorithms described by Equations (1), (4), and (5) describe tract bending functions that force a specific behavior upon the trajectory based upon certain properties about the tensor field (e.g., anisotropy, tensor orientation). Other bending functions may have even more optimized properties that enable crossing at oblique angles while maintaining the ability to follow highly curved trajectories.

One application of tractography is to parse out specific pathways for specific brain circuits. This is important for improving the understanding of the network of brain connections and how they vary across different population subgroups. Another exciting application is to map out the white matter trajectories in close proximity to brain tumors (or other lesions) for presurgical planning [Alexander et al., 1999; Witwer et al., 2002]. By mapping the relationship between white matter pathways and tumor, the impact of the surgery on white matter pathways can be assessed. A recent study by Holodny et al. [2001] used STT tracking to map out the corticospinal tract in relationship to the brain tumor prior to surgery. Eigenvector color maps [Makris et al, 1997; Pajevic and Pierpaoli, 1999] can also provide similar directional information in these cases [Witwer et al., 2002], but the typical colors associated with specific tracts will often be altered by changes in the white matter trajectories by the tumor presence. One case has been presented in this study, and other studies have shown similar abilities to track in proximity to brain tumors [e.g., Mori et al., 2001; Steijltes et al., 2001]. A mapping study of estimated white matter trajectories in brain tumor cases is currently being performed. Ideally, tractography using diffusion tensor image data will accurately represent the organizational architecture of white matter connections in the human brain. Unfortunately, it is very difficult to verify tractography maps of white matter connectivity in the living human brain. The complete patterns of connectivity and organization of white matter in the human brain is far from being elucidated and still under debate [Ture et al., 2000]. The current base of knowledge for white matter fiber anatomy has primarily been obtained by using fiber dissection and histology techniques in postmortem brain specimens [Glubenovich and Williams, 1980; Heimer, 1995; Krieg, 1966; Riley, 1960]. More complete studies have been done on animals, which can only be partially extrapolated to humans. The complexity of the underlying white matter organization is a significant challenge. Millions of white matter fibers merge into bundles and eventually fan out [Heimer, 1995]. In certain regions, the white matter structures may become interwoven. Obviously, this is a great challenge for diffusion tensor-based tractography techniques, since the size of the image voxel may be much larger than the structures of interest.

To date, reported tractography results (including those in this study) are unverified except by anecdotal comparisons with known anatomy. The challenge remains to verify the accuracy of these results using a variety of techniques including simulations [Lazar and Alexander, 2001; Lori et al., 2000], measurements on excised tissue specimens [Guilfoyle et al., 2001], axon labeling in animal models [Watanabe et al., 2001], and intraoperative mapping techniques [Penfield and Jasper, 1954].

ACKNOWLEDGMENTS

We thank John Roberts for useful discussions in software development, and Dennis Parker for valuable comments. Special thanks go to Larry Stensaas for useful discussions regarding the brain anatomy.

REFERENCES

Alexander AL, Burr RB, McDonald J, Hasan K, Jones G, Chong B, Tsuruda JS (1999): A technique for functional localization of the sensory motor cortex with diffusion anisotropy. In: Proc of the 7th Scientific Meeting of ISMRM, Philadelphia, p. 326.

Alexander AL, Hasan HM, Kindlmann G, Parker DL, Tsuruda JS (2000): A geometric analysis of diffusion anisotropy measures. Magn Reson Med 44:283–291.

Alexander AL, Hasan HM, Lazar M, Tsuruda JS, Parker DL (2001): Analysis of partial volume effects in diffusion-tensor MRI. Magn Res Med 45:770–780.

Anderson AW (2001): Theoretical analysis of the effects of noise on diffusion tensor imaging. Magn Reson Med 46:1174–1188.

Basser PJ, Pierpaoli C (1996): Microstructural and physiological features of tissues elucidated by quantitative-diffusion-tensor MRI. J Magn Reson B 111:209–219.

Basser PJ, Pierpaoli C (1998): A simplified method to measure the diffusion tensor from seven MR images. Magn Res Med 39:928–934.

Basser PJ, Pajevic S, Pierpaoli C, Duda J, Aldroubi A (2000): In vivo tractography using DT-MRI data. Magn Res Med 44:625–632.

Buonocore MH (1994): Estimation of total coronary artery flow using measurements of flow in the ascending aorta. Magn Reson Med 32:602–611.

Conturo TE, Lori NF, Cull TS, Akbudak E, Snyder AZ, Shimony JS, McKinstry RC, Burton H, Raichle ME (1999): Tracking neuronal fiber pathways in the living human brain. Proc Natl Acad Sci 96:10422–10427.

Gluhbegovic, N, Williams TH (1980): The human brain: a photographic guide. Hagerstown: Harper & Row; 176p.

Guilfoyle DN, Helpern JA, Lim KO (2001): Diffusion tensor imaging in fixed brain tissue. In: Proc 9th ISMRM Annual Meeting, Glasgow, p 1504.

Hasan KM, Parker DL, Alexander AL (2001): Comparison of gradient encoding schemes for diffusion-tensor MRI. J Magn Reson Imag 13:769–780.

Krieg WJS (1966): Functional neuroanatomy. Evanston, Ill: Brain Books, 874 p.

Heimer L. 1995. The human brain and spinal cord: functional neuroanatomy and dissection guide. New York: Springer-Verlag, 506 p.

Helman J, Hesselink L (1991): Visualizing vector field topology in fluid flows. IEEE Comput Graph Appl 11:36–46.

Holodny AI, Ollenschleger MD, Liu WC, Schulder M, Kalnin AJ (2001): Identification of the corticospinal tracts achieved using blood-oxygen-level-dependent and diffusion functional MR imaging in patients with brain tumors. AJNR 22:83–88.

Jones DK, Simmons A, Williams SCR, Horsfield MA (1999): Noninvasive assessment of axonal fiber connectivity in the human brain via diffusion tensor MRI. Magn Reson Med 42:37–41.

Kindlmann G, Weinstein D (1999): Hue-balls and lit-tensors for direct volume rendering of diffusion tensor fields. In: IEEE Visualization Proc, San Francisco, p 183–189.

Lazar M, Alexander AL (2001): Error analysis of white matter tracking algorithms (streamlines and tensorlines) for DT-MRI. In: Proc 9th ISMRM Annual Meeting, Glasgow, p. 506.

Lazar M, Weinstein D, Hasan KM, Alexander AL (2000): Axon tractography with tensorlines. In: Proc of the 8-th Scientific Meeting of ISMRM, Denver, p 482.

Lazar M, Hasan KM, Alexander AL (2001b): Bootstrap analysis of DT-MRI tractography techniques: streamlines and tensorlines. In: Proc 9th ISMRM Annual Meeting, Glasgow, p 1527.

Le Bihan D, Mangin JF, Poupon C, Clark CA, Pappata S, Molko N, Chabriat H (2001): Diffusion tensor imaging: concepts and applications. J Magn Reson Imaging 13:534–546.

Lori NF, Akbudak E, Snyder AZ, Shimony JS, Conturo TE (2000): Diffusion tensor tracking of human neuronal fiber bundles: simulation of effects of noise, voxel size, and data interpolation. In: Proc of the 8-th Scientific Meeting of ISMRM, Denver, p 775.

Makris N, Worth AJ, Sorensen AG, Papadimitriou GM, Wu O, Reese TG, Wedeen VJ, Davis TL, Stakes JW, Caviness VS, Kaplan E, Rosen BR, Pandya DN, Kennedy DN (1997): Morphometry of in vivo human white matter association pathways with diffusion-weighted magnetic resonance imaging. Ann Neurol 42:951–962.

Mori S, Crain B, Chacko VP, van Zijl PCM (1999): Three dimensional tracking of axonal projections in the brain by magnetic resonance imaging. Ann Neurol 45:265–269.

Mori S, Kraut MA, van Zijl PC, Solaiyappan M, Brem H, Pomper M (2001): Diffusion tensor imaging and fiber tracking of brain tumors. In: Proc 9th ISMRM Annual Meeting, Glasgow, p 507.

Mori S, Kaufmann WE, Davatzikos C, Stieljes, Amodei L, Fredericksen K, Pearlson GD, Melhem ER, Solaiyappan M, Raymond GV, Moser HW, van Zijl PC (2002): Imaging cortical association tracts in the human brain using diffusion-tensor-based axonal tracking. Magn Reson Med 47:215–223.

Napel S, Lee DH, Frayne R, Rutt BK (1992): Visualizing three-dimensional flow with simulated streamlines and three-dimensional phase-contrast MR imaging. J Magn Reson Imaging 2:143–153.

Pajevic S, Pierpaoli C (1999): Color schemes to represent the orientation of anisotropic tissues from diffusion tensor data: application to white matter fiber tract mapping in the human brain. Magn Reson Med 42:526–540.

Penfield W, Jasper HH (1954): Epilepsy and the functional anatomy of the human brain. Boston: Little Brown, 896 p.

Pierpaoli C, Basser PJ (1996): Toward a quantitative assessment of diffusion anisotropy. Magn Res Med 36:893–906.

Poupon C, Clark CA, Frouin V, Regis J, Bloch I, Le Bihan D, Mangin J (2000): Regularization of diffusion-based direction maps for the tracking of brain white matter fascicles. Neuroimage 12:184–195.

Riley HA (1960): An atlas of the basal ganglia, brain stem and spinal cord, based on myelin-stained material. New York: Hafner Pub. Co. 708 p.

Stieltjes B, Kaufmann WE, van Zijl PCM, Fredericksen K, Pearlson GD, Solaiyappan M, Mori S (2001): Diffusion tensor imaging and axonal tracking in the human brain. Neuroimage 14:723–735.

Tench CR, Morgan PS, Wilson M, Blumhardt LD (2002): White matter mapping using diffusion tensor MRI. Magn Reson Med 47:967–972.

Tuch DS, Weisskoff RM, Belliveau JW, Wedeen VJ (1999): High angular resolution diffusion imaging of the human brain. In: Proc 7th Annual ISMRM, Philadelphia, p 321.

Ture U, Yasargil MG, Friedman AH, Al-Mefty O (2000): Fiber dissection technique: lateral aspect of the brain. Neurosurgery 47: 417–426.

Watanabe T, Michaelis T, Frahm J (2001): In vivo 3D imaging of the rat visual pathway using Mn2+ as a tract tracer. In: Proc 9th ISMRM Annual Meeting, Glasgow, p 1493.

Wedeen VJ, Reese TG, Tuch DS, Weigel MR, Dou JG, Weisskoff RM, Chessler D (2000): Mapping fiber orientation spectra in cerebral white matter with Fourier transform diffusion MRI. In: Proc 8th ISMRM Annual Meeting, Denver, p 82.

Weinstein DM, Kindlmann GL, Lundberg EC (1999): Tensorlines: advection-diffusion based propagation through diffusion tensor fields. In: IEEE Visualization Proc, San Francisco, p 249–253. [http://www.sci.utah.edu/publications/vis99_tensorlines-paper.pdf]

Westin CF, Maier SE, Khidir B, Everett P, Jolesz FA, Kikinis R (1999): Image processing for diffusion tensor magnetic resonance imaging. In: Taylor C, Colchester A, editors. Lecture notes in computer science: medical image computing and computed-assisted intervention. Cambridge: Springer. p 441–452.

Wiegell MR, Larsson HB, Wedeen VJ (2000): Fiber crossing in human brain depicted with diffusion tensor MR imaging. Radiology 217:897–903.

Witwer BP, Moftakhar R, Hasan KM, Praveen D, Arfanakis K, Haughton V, Rowley H, Field A, Noyes J, Meyerand ME, Alexander AL, Badie B (2002): Diffusion tensor imaging of white matter tracts in patients with cerebral neoplasms. J Neurosurg 97:568–575.

Woods RP, Grafton ST, Holmes CJ, Cherry SR, Watson J, Mazziotta JC (1998): Automated image registration:I. General methods and intrasubject, intramodality validation. J Comput Assist Tomogr 22:141–154.

Xue R, van Zijl PCM, Crain BJ, Solaiyappan M, Mori S (1999): In vivo three-dimensional reconstruction of rat brain axonal projections by diffusion tensor imaging. Magn Res Med 42:1123–1127.